

Dual AGNs on 100 kpc Scales from the Million Quasar Catalog

ZHUOJUN DENG ^{1,2,*} CHENG XIANG ^{1,2,*} QIHANG CHEN ^{1,2} LIANG JING ^{1,2} XINGYU ZHU ^{1,2} AND
JIANGHUA WU^{†1,2}

¹*School of Physics and Astronomy, Beijing Normal University, Beijing 100875, China*

²*Institute for Frontier in Astronomy and Astrophysics, Beijing Normal University, Beijing, 102206, China*

ABSTRACT

Research on dual active galactic nuclei (AGNs) is crucial for understanding the coevolution of galaxies and supermassive black holes. However, the current number of dual AGNs remains scarce. In this work, we selected 173 new dual AGNs, 4 AGN triplets, and 1 AGN quadruplet from the Million Quasars Catalog, all with low redshift ($z < 0.5$), a projected distance (r_p) of no more than 100 kpc, and a line-of-sight velocity difference ($|\Delta v|$) of less than 600 km s⁻¹, thus supplementing existing low-redshift dual AGNs demographics. Visual inspection of the optical images from the Dark Energy Spectroscopic Instrument Legacy Survey was performed for each pair, revealing that $\sim 16\%$ of pairs exhibit tidal features. Statistical analyses show an increasing number of dual AGNs with decreasing redshift, with velocity difference primarily at $|\Delta v| < 300$ km s⁻¹, which is likely an artifact of our selection strategy. The tidal sample peaks as having 13 pairs at $5\text{-}20h_{70}^{-1}$ kpc, but drops to 1 pair $> 55h_{70}^{-1}$ kpc. Our study also explores the wide separation ($r_p > 10$ kpc) dual AGNs, finding 165 such systems, with 25 displaying clear tidal features. Furthermore, some extra galaxies, AGNs, and/or their candidates were found in the same regions of the pairs or multiplets forming interacting systems with these pairs or multiplets.

Keywords: Black hole physics (1879) — Galaxies (573) — Interactions galaxies (600) — Active galactic nuclei (16)

1. INTRODUCTION

Galaxy interactions and mergers have long been recognized as critical factors in shaping the structure and morphology of galaxies (F. Zwicky 1956; A. Toomre & J. Toomre 1972; D. B. Sanders et al. 1988; J. E. Barnes & L. Hernquist 1992; J. M. Lotz et al. 2008; C. J. Conselice 2014). They usually manifest themselves as dual or even multiple cores, irregular galactic morphologies, gas bridges or rings, and tidal tails. These interactions cause the galactic gas to lose angular momentum and to move towards the galactic center (J. E. Barnes & L. Hernquist 1996; T. J. Cox et al. 2008; K. A. Blumenthal & J. E. Barnes 2018). If the gas can reach the supermassive black holes (SMBHs), they can begin fueling as active galactic nuclei (AGNs) (J. Kormendy 2013; P. F. Hopkins & E. Quataert 2010); otherwise, the gas may instead trigger starburst activity (T. Di Matteo et al. 2005; P. F. Hopkins et al. 2008; T. J. Cox et al. 2008).

The study of dual AGNs in galaxy mergers is of great importance to various astrophysical inquiries. They provide unique laboratories for the investigation of galaxy evolution, star formation, the growth and evolution of SMBHs, and the eventual emission of gravitational waves (P. F. Hopkins et al. 2006; G. Kauffmann & M. Haehnelt 2000; T. Di Matteo et al. 2005). SMBH pairs are thought to be a generic outcome in the hierarchical paradigm of structure formation (M. C. Begelman et al. 1980; M. Milosavljević & D. Merritt 2001; Q. Yu 2002), given that most massive galaxies harbor SMBHs (J. Kormendy & D. Richstone 1995; D. Richstone et al. 1998). Both SMBHs in a merger may accrete at the same time, which will be observable as a pair of AGNs. Those pairs with separations of individual members < 100 kpc are also frequently referred to as "dual AGNs" (A. D. Rosa et al. 2019; R. W. Pfeifle et al. 2025). However, it is difficult to predict when one, and especially both, SMBHs become active (I. Shlosman et al. 1990; P. J. Armitage & P. Natarajan 2002; K. Wada 2004; M. Dotti et al. 2007, 2012). The frequency of dual AGNs can constrain models involving galaxy merger rates and tidally triggered

Email: jhwu@bnu.edu.cn

* Co-author with equal contribution.

AGN activity (Q. Yu et al. 2011; A. Foord et al. 2024). The properties of their host galaxies offer clues about the external and internal conditions that enable both SMBHs to become active (P. F. Hopkins et al. 2008; L. Blecha et al. 2013). When two galaxies merge, their SMBHs sink via dynamical friction, form a bound binary, harden, and finally coalesce (M. C. Begelman et al. 1980). The merger of binary SMBHs is anticipated to produce low-frequency gravitational waves (D. J. Reardon et al. 2023; EPTA Collaboration et al. 2024), the detection of which would directly test the theory of general relativity and allow for the exploration of SMBH populations in the early universe (S. W. Hawking & W. Israel 1987; M. G. Haehnelt 1994; D. E. Holz & S. A. Hughes 2005; Z. Arzoumanian et al. 2020; P. Amaro-Seoane et al. 2023).

There have been an increasing number of studies that identified dual AGNs with separations ranging from < 1 kpc to tens of kpc in the X-ray (S. Komossa et al. 2003; L. Ballo et al. 2004; S. Bianchi et al. 2008; E. Piconcelli et al. 2010; K. Iwasawa et al. 2011; M. Koss et al. 2012; M. J. Koss et al. 2016), radio (F. N. Owen et al. 1985; C. Rodriguez et al. 2006; H. Fu et al. 2011b), and optical (A. D. Myers et al. 2006, 2007; J. M. Comerford et al. 2009b; J. F. Hennawi et al. 2006; J. F. Hennawi et al. 2010; X. Liu et al. 2010a; X. Liu et al. 2011b) bands. Moreover, several tens of quasar pairs have also been discovered as byproducts of gravitational lensing searches (N. Inada et al. 2012; C. A. Lemon et al. 2018; M. Yue et al. 2023; F. Dux et al. 2024). Due to the extensive sky coverage, wide wavelength range, high data quality, and rich sample of Sloan Digital Sky Survey (SDSS) spectra, the SDSS is commonly used to systematically identify and analyze dual AGN candidates. A subset of systems on the kpc scale identified in SDSS spectra has been further confirmed through high-resolution near-infrared(NIR) imaging (D. J. Rosario et al. 2011; Q. Wang et al. 2025) and spatially resolved optical spectroscopy (X. Liu et al. 2010a; H. Fu et al. 2012a).

These objects were initially identified through the “double-peak” selection method (J.-M. Wang et al. 2009; X. Liu et al. 2010; Z.-X. Shi et al. 2014; L. Wang et al. 2017), which searches for double-peaked emission-line profiles as indicators of dual nuclei. However, this method exhibits two limitations: firstly, due to the limited resolution of SDSS spectra, it is biased against pairs with line-of-sight (LOS) velocity differences smaller than approximately 150 km s^{-1} (X. Liu et al. 2010a; X. Liu et al. 2010). Secondly, it is biased against pairs with separations larger than a few kpc, as pairs with angular distances greater than $3''$ (the diameter of an SDSS fiber) cannot fit within a single SDSS fiber.

To circumvent the limitations of the double-peak method and establish a larger sample of dual AGNs at low redshift, X. Liu et al. (2011b) adopted complementary methods to identify AGN pairs at $\bar{z} \sim 0.1$ from SDSS DR7. They assembled a sample of 1286 dual AGNs and candidates, 30% of which show morphological tidal features in SDSS optical images. In recent years, the number of AGNs and quasars has significantly increased. R. W. Pfeifle et al. (2025) presented the Big Multi-AGN Catalog (The Big MAC) DR1, which includes 156 confirmed dual AGNs and 4180 dual AGN candidates, compiled from hundreds of literature articles published between 1970 and 2020. As of June 2023, the Million Quasar Catalog (MQC, version 8.0; E. W. Flesch 2023) has cataloged 1,021,800 quasars and candidates. This provides new possibilities for further exploration of low-redshift dual AGNs.

We conducted a systematic search for multiple AGN systems within the range of $0 < z < 0.5$ in the MQC, limiting the projected distance to $r_p < 100h_{70}^{-1}$ kpc and the LOS velocity difference to $|\Delta v| < 600 \text{ km s}^{-1}$. The latter two selection criteria were proposed by J. D. Silverman et al. (2011); X. Liu et al. (2011b). These criteria are also consistent with prior works and definitions for dual AGNs (M. Koss et al. 2011, 2012; A. D. Rosa et al. 2019), and this is similar to the dual AGN criteria recently laid out by R. W. Pfeifle et al. (2025). The objective is to identify new multiple AGN systems at low redshifts, and to study the characteristics of dual AGNs in order to understand the process of galaxy mergers and their impact on galaxy evolution.

This paper is organized as follows: In Section 2, the data and the method of sample selection are described. We present images of dual AGNs from the Ninth or Tenth Data Release of the Dark Energy Spectroscopic Instrument Legacy Survey³ (DESI-LS; A. Dey et al. (2019)). In Section 3, we examine the frequency of dual AGNs with tidal features and provide preliminary statistics of these pairs. Section 4 and 5 give the discussion on the implications of our results and the conclusions. Throughout, a Λ -cold dark matter (Λ CDM) cosmology is assumed with $\Omega_m = 0.3$, $\Omega_\Lambda = 0.7$, and $H_0 = 70 \text{ km s}^{-1}\text{Mpc}^{-1}$.

2. DATA AND SAMPLE SELECTION

2.1. Data

All of our objects come from the MQC, Version 8, which contains 907,144 type-I QSOs and AGNs. 66,026 QSO candidates are also included, calculated via

³ <https://www.legacysurvey.org/acknowledgment/>

radio/X-ray association (including double radio lobes) with a confidence level of 99%. Including blazars and type II objects increases the total number of AGNs to 1,021,800. Compared to previous studies of dual AGNs (X. Liu et al. 2011b; M. Koss et al. 2012), our parent sample is larger by several orders of magnitude, but it is intrinsically heterogeneous and drawn from a variety of surveys. Therefore, it is important to give a detailed description of its classification scheme and redshift assignments, which are directly relevant to the construction of our sample.

In the MQC, sources classified as Q (QSO, broad-line nucleus-dominated quasars), A (AGNs, broad-line Seyferts/host galaxy-dominated AGNs), K (narrow-line QSO), and N (narrow-line Seyfert) are all assigned spectroscopic redshifts. For B-class objects (BL Lac type), redshift information is not required and may therefore be absent, or represented by a photometric redshift with a typical precision of ~ 0.1 . More than 90% of the AGNs in our sample consist of broad-line and narrow-line Seyfert populations, which are mainly drawn from the PGC⁴ and SDSS DR16 catalogs. We emphasize that, given the MQC inclusion rules, it is appropriate to describe our working sample drawn from MQC as spectroscopically confirmed: when literature samples mix spectroscopic and photometric redshifts, MQC retains only spectroscopic quasars as classified objects to ensure reliable classifications and redshifts (E. W. Flesch 2023). Accordingly, all sources in our sample have spectroscopic redshifts. Note that MQC uses a broad “AGN” label and does not distinguish Seyferts, LINERs, and Composites. Thus, we assume LINERs and Composites represent AGNs, consistent with X. Liu et al. (2011b). Although some LINERs/Composites may in fact not host actively accreting SMBHs, we assume that these systems are accreting SMBHs in this work.

In addition, the suffixes R (radio), X (X-ray), and 2 (double radio lobes) indicate that the source has been associated with detections in the corresponding bands, based on the Millions of Optical-Radio/X-ray Associations (MORX) catalogue (E. W. Flesch 2024). The latest MORX v2 release evaluates associations from all the largest radio and X-ray surveys to June 2023, including VLASS, LoTSS, RACS, FIRST, NVSS, and SUMSS in radio, and Chandra, XMM-Newton, Swift, and ROSAT in X-rays (E. W. Flesch 2024). These associations are based on optical-radio/X-ray cross-matching probabilities, derived by comparing the areal densities of optical profiles around radio/X-ray detections to back-

ground averages (E. Flesch & M. J. Hardcastle 2004). It should be noted that composite labels in the MQC (e.g., AR, NX, NR2) primarily indicate the availability of multiwavelength observations (radio/X-ray/double radio lobes) and do not alter the intrinsic physical classification of the source, nor do they imply that the objects are bona fide radio/X-ray AGNs.

For consistency and to simplify the statistical analysis, we adopt the following classification scheme: (1) sources labeled with “Q” (e.g., Q, QR, QRX, QX) are uniformly classified as QSOs; (2) sources labeled with “A” (e.g., A, AR, AX, ARX, AR2, AR2X) are grouped into the AGN category (broad-line Seyfert-type AGNs); (3) sources whose class string begins with “B” (e.g., B, BR, BX, BRX, B2) are classified as BL Lac objects (FSRQs are instead typed as QSOs); (4) sources labeled with “K” or “KX” are grouped into the NLQSO class (type-II narrow-line QSOs); (5) sources labeled with “N”, “NR”, “NRX”, “NX”, or “NR2” are grouped into the NLAGN class (narrow-line Seyfert-type or host-dominated AGNs). The majority of these narrow-line objects in our sample originate from SDSS DR16, but a non-negligible fraction are drawn from other spectroscopic surveys such as 2dF, 2SLAQ, and the Principal Galaxies Catalogue (PGC).

Our optical imaging data are from DESI-LS, a project dedicated to constructing a comprehensive map of the sky through optical and infrared imaging observations. These images were used in the visual examination of our sample in the optical band, specifically in identifying the signs of galaxy interactions. In comparison to SDSS and the Panoramic Survey Telescope and Rapid Response System (Pan-STARRS), DESI-LS stands out for its extensive depth and coverage, making it superior for tasks such as galaxy morphological classification.

2.2. Sample Selection

Our sample of dual AGNs was selected based on three criteria: (1) The redshift cut of $0 < z < 0.5$, (2) The projected distance between individual members of $r_p < 100 h_{70}^{-1}$ kpc, and (3) the line of sight (LOS) velocity difference between members of $|\Delta v| < 600 \text{ km s}^{-1}$ (J. D. Silverman et al. 2011; X. Liu et al. 2011b). The choice of $100 h_{70}^{-1}$ kpc is somewhat larger than the typical thresholds adopted in galaxy pair studies (E. J. Barton et al. 2000; S. L. Ellison et al. 2008; D. W. Darg et al. 2010), but is comparable to the lower limit of the galaxy pairwise velocity dispersion measured at projected distances of $150 \leq r_p \leq 5000 h_{70}^{-1}$ kpc (I. Zehavi et al. 2002).

We first applied criterion (1) to select 103,216 AGNs with redshifts $z < 0.5$ from the MQC as our initial sample. Based on their redshifts, we calculated the pro-

⁴ <https://heasarc.gsfc.nasa.gov/W3Browse/all/pgc2003.html>

jected distance corresponding to $100 h_{70}^{-1}$ kpc according to the criterion (2). The initial sample was then self-matched with TOPCAT (M. B. Taylor 2005), adopting the maximum angular separation as the matching radius. From the self-matched results, we extracted candidate pairs satisfying criterion (2), and subsequently calculated their LOS velocity differences ($|\Delta v|$) following D. W. Hogg (2000). Applying criterion (3), we identified 319 dual AGN candidates. To exclude previously known systems, we cross-matched these candidates against several comprehensive dual AGN catalogs (M. Koss et al. 2011, 2012; X. Liu et al. 2011b; Y.-W. Zhang et al. 2021; Y.-C. Chen et al. 2023; R. W. Pfeifle et al. 2025) and also checked the Simbad database⁵ (M. Wenger et al. 2000) for possible duplicates in recent years. This left us with 184 candidate systems. We then visually inspected the optical images of DESI-LS, rejecting six false pairs and identifying five multiplets (four triplets and one quadruplet). Finally, our sample comprises 178 systems: 173 dual AGNs, 4 triplets, and 1 quadruplet. The basic properties of all systems are summarized in Table 1.

2.3. Dual AGNs with Tidal Features

We then derived a subset of dual AGN candidates residing in galaxy mergers unambiguously experiencing strong tidal encounters. The selection was made through visual inspection of DESI-LS optical images (DR9 *grz* and DR10 *griz*), focusing on systems exhibiting tidal features such as bridges, tails, shells, or rings. We use visual examination for several reasons: (1) Visual inspection is more sensitive to low surface brightness (LSB) features such as bridges, tails, shells, and rings. These features are often critical for identifying tidal interactions but can be challenging to detect with automated techniques. (2) Compared to automated techniques like model fitting, visual identification is less prone to false positives. This means that we are less likely to misidentify misleading or elusive features as real tidal interactions. (3) While quantitative measures of mergers, such as those by C. J. Conselice (2003) and J. M. Lotz et al. (2004), are more objective and can produce reproducible results, they may introduce biases towards certain merger stages. For instance, these measures may be susceptible to the first pericenter passage or the final coalescence of merging galaxies, as noted by J. M. Lotz et al. (2008). Visual identification helps mitigate these biases by providing a more comprehensive assessment of tidal features across different stages of the merger process (X. Liu et al. 2011b). To reduce the uncertainty of the visual inspection, two of our members (Z.J.D. and

C.X.) independently inspected each pair three times, without knowing the results from previous identifications. 98% of the trial results were consistent, for objects with different classifications, the category assigned in the majority of the trials (two out of three occurrences) was adopted as the final classification.

We identified 27 dual AGNs with tidal features in the optical images. Figure 1 shows representative examples of these systems, where the optical morphologies display prominent tidal tails, bridges, or distorted isophotes suggestive of ongoing galaxy interactions. In some systems (e.g., J0103+0029, J1426+0209, J1626+4340), only marginally extended or asymmetric structures are visible, making it difficult to identify more prominent bridge- or ring-like features. We also look forward to obtaining more images at declinations below -30° in the future to identify additional tidal systems.

3. SAMPLE STATISTICS AND RESULTS

Our systematic search and analysis in the MQC has led to the identification of 178 new multi-AGN systems at low redshifts ($z < 0.5$), which include 173 pairs, 4 triplets, and 1 quadruplet, all with $r_p < 100 h_{70}^{-1}$ kpc and $|\Delta v| < 600$ km s⁻¹. Here we present some results and statistics on these AGN systems. The optical images of the dual AGNs are presented in the Appendix 5. For each system, three panels are shown from left to right: the DESI-LS DR10 image, the DESI-LS DR10 model image, and the DESI-LS DR10 residual image. These images provide a clear visual representation of the morphological characteristics of the sources in our sample and the results of the model fitting.

3.1. Statistics and Analysis of Dual AGNs

MQC is an inhomogeneous catalog that compiles AGNs from multiple surveys with varying target selection criteria, spectral quality, and data completeness. Such differences may influence our statistical analyses, similar to the systematic band- and technique-dependent biases emphasized in the Big MAC DR1 study (R. W. Pfeifle et al. (2025), Section 4).

Our data consist of 346 individual AGNs within 173 dual systems. Figure 2 shows the redshift distribution of various source types in our dual AGN sample. This distribution suggests that, among low-redshift dual AGN systems in the MQC, the majority are low-luminosity galaxies, predominantly narrow-line AGNs (56.1%) and Seyfert-type broad-line AGNs (34.1%). In contrast, QSOs, BL Lacs, and radio-loud AGNs/FSRQs are relatively rare, together comprising only about 5%. Table 2 provides detailed statistics on the classification combinations in our dual AGN samples. BL Lac objects and

⁵ SIMBAD database: <https://simbad.u-strasbg.fr/simbad/>

Table 1. Catalog of dual AGNs in this work (system-based format).

Obj. Name	RA(A) (J2000)	Dec(A) (J2000)	RA(B) (J2000)	Dec(B) (J2000)	z_A	z_B	$\Delta\theta$ ($''$)	r_p (h_{70}^{-1} kpc)	Δv (km s $^{-1}$)	r_A (mag)	r_B (mag)	Class(A,B)	Cite	F_{tidal}
J0018-0045	4.511177	-0.75948	4.51300	-0.74598	0.0636	0.0640	48.79	59.74	98.96	17.18	17.10	N, A	DR16, 6dF	N
J0103+0029	15.81653	0.48763	15.81621	0.48838	0.2021	0.2025	2.94	9.77	110.79	20.19	17.89	N, N	DR16, DR16	T
J0113-1450	18.45865	-14.84566	18.45771	-14.84919	0.0520	0.0540	13.15	13.34	569.80	10.09	14.03	ARX, N	1237, 6dF	T
J0114-5523	18.59292	-55.39700	18.60388	-55.39705	0.0120	0.0122	22.42	5.51	58.16	8.41	12.67	N, NRX	930, 6dF	T
J0120-0829	20.19541	-8.49063	20.20007	-8.48844	0.0340	0.0344	18.36	12.45	110.23	13.15	12.53	N, NRX	PGC, PGC	T
J0120-4407	20.04900	-44.13282	20.08202	-44.12858	0.0221	0.0234	86.65	38.79	372.89	10.25	6.70	NX, NRX	PGC, PGC	T
J0457-7527	74.42021	-75.45917	74.34222	-75.44512	0.0179	0.0190	86.79	30.69	473.43	6.74	4.94	NX, N	PGC, PGC	N
J0852+4121	133.24919	41.36016	133.24631	41.36751	0.1342	0.1348	27.68	65.66	149.67	15.63	16.81	AR, AR2	DR16, DR16	N
J1014+0327	153.56228	3.46658	153.44030	3.42467	0.0030	0.0040	463.57	28.77	298.95	5.88	5.8	ARX, NRX	1592, PGC	N
J1612+2934	243.04692	29.57412	243.06965	29.57306	0.0536	0.0542	71.26	74.41	165.10	8.83	12.81	ARX, NRX	PGC, PGC	N
J2254+0046	343.71762	0.77538	343.71429	0.77648	0.0908	0.0913	12.64	21.39	123.74	16.82	15.68	QR, N	DR16, DPeake	T
J2353-3036	358.49433	-30.60231	358.49467	-30.60008	0.3134	0.3144	8.06	37.02	228.33	19.28	19.52	QR, N	2QZ, 2QZ	N

NOTE.—Columns: (1) System name; (2–5) Right ascension and declination (degrees) of components A and B; (6–7) Spectroscopic redshifts of A and B; (8–10) Angular separation, projected distance, and the LOS velocity difference; (11–12) r -band magnitude of A and B; (13) Classifications given by the MQC, see Section 2.1 for details; (14) Reference to the original discoveries, cite numbers correspond to the Miliquas reference list^a. And most of these sources originate from small-scale follow-up observations with non-survey telescopes; (15) Tidal feature flag ("T" = tidal pair, "N" = non-tidal pair).
(This entire table is available in machine-readable form.)

^a<https://www.quasars.org/miliquas-references.txt>

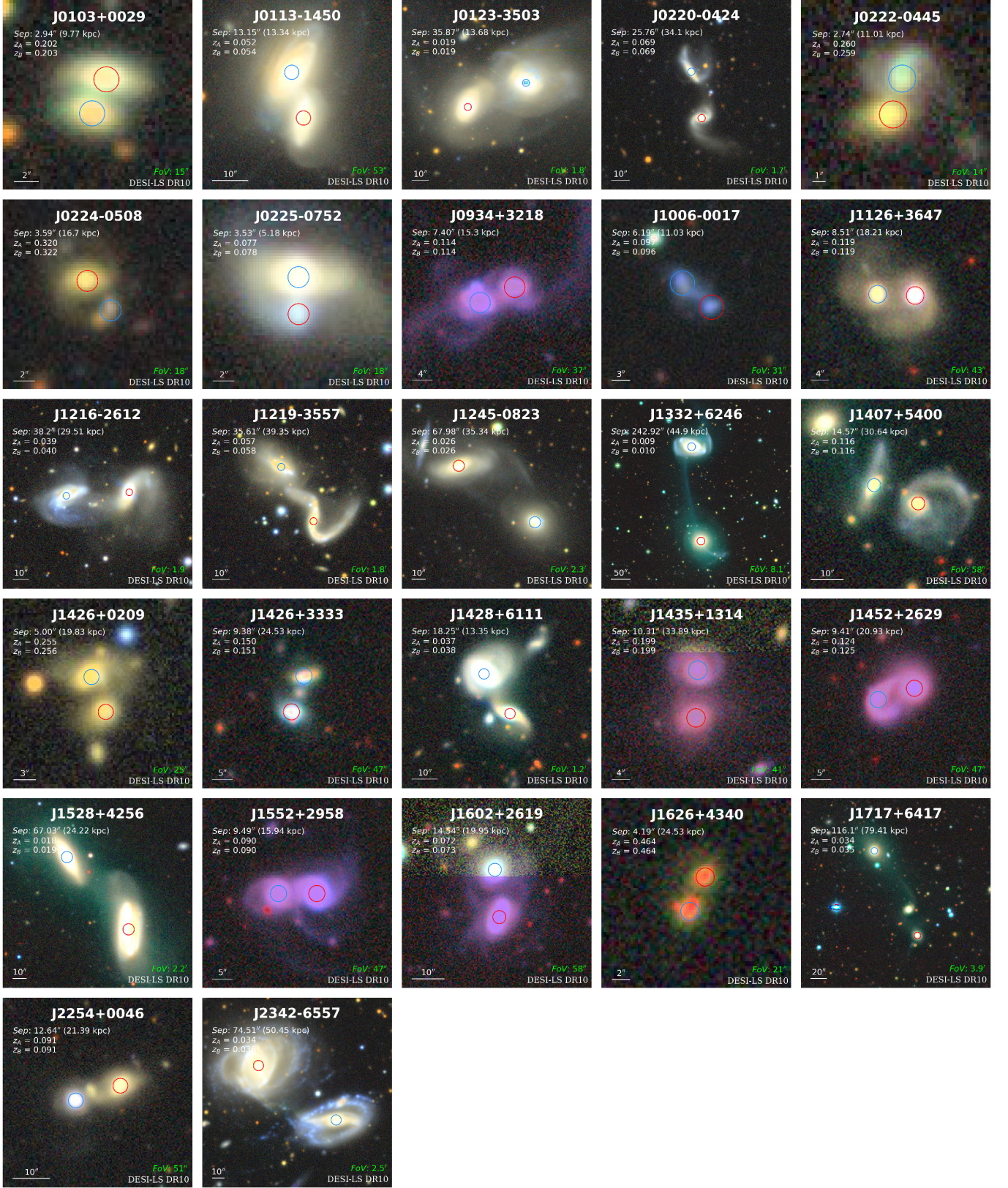


Figure 1. DESI–LS *grz(i)* images of each tidal system, showing clear tidal features associated with dual AGNs. Red and blue circles mark the locations of the AGNs. North is up and east is to the left. The field of view (FOV) of each image is labeled at the bottom right corner. The redshifts, r_p , and angular separation of each pair are also presented. The pinkish appearance in some images is likely due to incomplete band coverage.

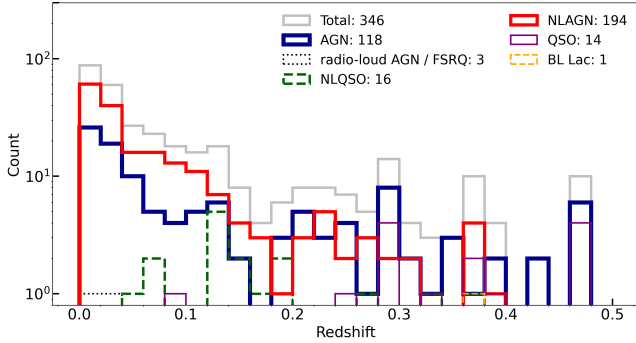


Figure 2. Redshift distribution of various types of sources in dual AGN sample.

broad-line radio-loud AGNs/FSRQs are combined into a single ‘blazar’ category for statistical purposes, following the conventional classification of blazars (C. M. Urry & P. Padovani 1995). The results show that AGN-NLAGN (35.3%) and NLAGN-NLAGN (35.8%) pairs dominate our sample, together accounting for more than 70% of all dual AGNs. This indicates that narrow-line AGNs make up the majority of low-redshift dual AGN systems. Such a trend is broadly consistent with the results of X. Liu et al. (2011b) on dual AGNs, who reported that narrow-line AGNs constitute up to 96% of their sample. In addition, the AGN-AGN combination of broad-line Seyfert AGNs also represents a significant fraction (14.5%). In contrast, quasar combinations (e.g., QSO-QSO at 1.7%, AGN-QSO at 2.9%, and NLAGN-QSO at 1.7%) are relatively rare, likely reflecting the scarcity of dual quasars at low redshifts. In addition, combinations with blazars or blazar-NLQSO are extremely rare, together accounting for only ~ 1 –2% of the sample.

Moreover, we identified 27 pairs with tidal features in optical images, corresponding to approximately 16% of our AGN sample. A subset of these systems is marked with a ‘T’ flag in Table 1 to explicitly indicate their tidal morphology. As a comparison, X. Liu et al. (2011b) visually inspected SDSS images and found that $\sim 30\%$ of their 1286 pairs showed tidal features, markedly higher than our result. It is a bit surprising that we found a much lower proportion of systems with tidal features despite having much deeper images. The tidal sample may lack mergers in their earliest stages prior to the first pericenter passage, as such events lack observable tidal features (A. Toomre & J. Toomre 1972). Furthermore, the strength of tidal signatures is influenced by the properties of the host galaxies and orbital parameters of the progenitor systems. While gas-rich major mergers on prograde orbits may readily generate strong tidal features (J. E. Barnes & L. Hernquist 1996; T. J. Cox et al. 2008), other merger populations lack-

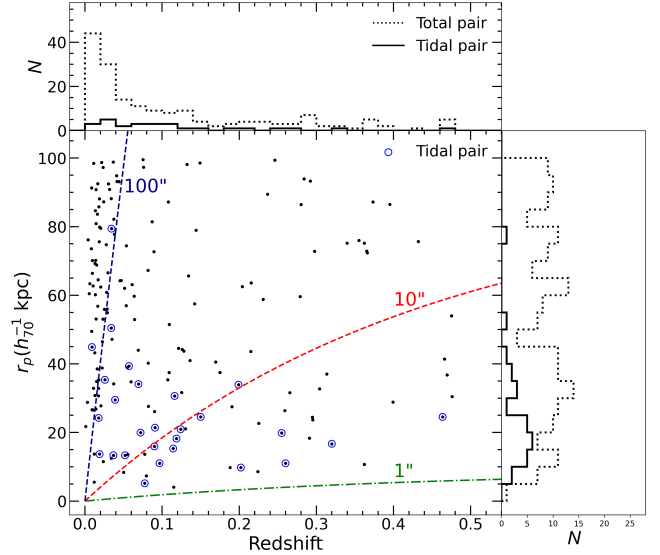


Figure 3. Projected distance (r_p) vs. redshift for our dual AGNs. Black dots represent all dual AGNs, while blue circles represent dual AGNs with identified morphological tidal features identified in the optical images. The dotted histograms represent the distributions of the full dual AGN sample, while the solid histograms show the distributions of the tidal sample. The green, red, and blue dashed lines correspond to angular separations of $1''$, $10''$, and $100''$, respectively.

ing discernible optical tidal features may consist of minor mergers with mass ratios exceeding 30 (J. M. Lotz et al. 2010), spheroidal mergers characterized by high bulge-to-disk ratios (J. C. Mihos & L. Hernquist 1996), and mergers occurring on highly retrograde orbits (A. Toomre & J. Toomre 1972).

Figure 3 shows the distribution of projected distance versus redshift for our sample. The number of dual AGNs increases toward lower redshifts. This redshift distribution is very likely a systematic effect driven by the selection methodology for MQC samples. For projected distance, the number is more evenly distributed. But in some bins, such as $45 \leq r_p \leq 50 h_{70}^{-1}$ kpc, contain relatively few systems, which may be due to the inhomogeneity of the parent sample. Similarly, the number of systems within $0 \leq r_p \leq 5 h_{70}^{-1}$ kpc is relatively lower, likely reflecting the angular resolution limits of the surveys. The tidal subsample is mainly concentrated at $z < 0.14$, and have separations in the range of $0 - 55 h_{70}^{-1}$ kpc. As r_p decreases, the number of tidal systems apparently increases, peaking at $10 - 20 h_{70}^{-1}$ kpc.

Figure 4 shows the distribution of the LOS velocity differences $|\Delta v|$ for our dual AGNs. The distribution shows a decreasing trend with increasing $|\Delta v|$. When $|\Delta v| > 400 \text{ km s}^{-1}$, the full and tidal samples contain

Table 2. Statistical analysis of classification combinations in the dual AGN sample

combination	Count	%	combination	Count	%	combination	Count	%
AGN-NLAGN	61	35.3	NLAGN-NLAGN	62	35.8	NLQSO-AGN	2	1.2
AGN-AGN	25	14.5	NLQSO-NLQSO	5	2.9	Blazar-NLAGN	2	1.2
AGN-QSO	5	2.9	NLQSO-NLAGN	4	2.3	Blazar-Blazar	1	0.6
QSO-QSO	3	1.7	NLAGN-QSO	3	1.7			

NOTE—Percentages are computed with respect to the full dual-AGN sample ($N = 173$).

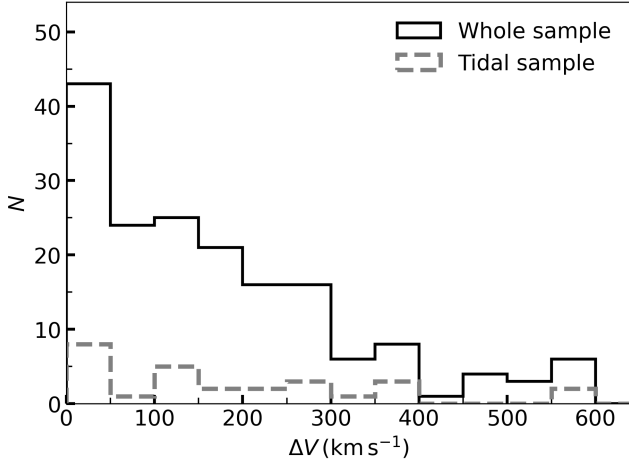


Figure 4. Distribution of LOS velocity difference $|\Delta v|$ for our dual AGNs. The black histogram represents the distribution of all dual AGNs, while the dark blue dashed line shows the distribution of the tidal sample.

only a small number of systems (15 dual AGNs in total, of which 3 are tidal systems). Notably, there is a drop-off in the number of pairs with $|\Delta v| > 300 \text{ km s}^{-1}$. The selection effect of the MQC might play some sort of role in the behavior of the distribution, this drop is consistent with that seen by (X. Liu et al. 2011b). For the tidal subsample, no clear trend is observed due to the limited number of systems.

3.2. Close- and Wide-Separation Systems

At small angular separations, we identified a dual AGN candidate, J1053+4710, with a projected distance of $r_p < 5 h_{70}^{-1} \text{ kpc}$ and an angular separation of $1.961''$. The residual image shown in Appendix 5 further reveals two prominent nuclei. However, the emission line strengths and continuum levels of the two spectra appear similar in Figure 5. A more critical issue for such close pairs drawn from fiber surveys is fiber spillover. For our sample, close angular pairs with separations $< 10''$ may suffer from such spillover effects, meaning some emission from both nuclei could be contained in both fibers. This complicates the definitive spectroscopic confirma-

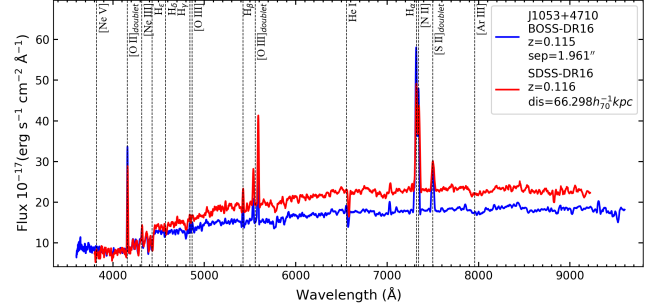


Figure 5. Comparison of SDSS and BOSS spectra for the dual AGN system J1053+4710. Major emission lines are marked with vertical dashed lines, and the basic properties of the two components are shown in the upper-right corner.

tion based on the survey data alone. Therefore, these close pairs, including J1053+4710, should be considered as dual AGN candidates and require spatially resolved follow-up spectroscopy for verification.

Furthermore, we define those pairs with $r_p > 10 h_{70}^{-1} \text{ kpc}$ as wide separation dual AGNs (WSAPs). Our sample includes 165 WSAPs, with 25 displaying clear tidal features, which are shown in Figure 1. Figure 6 illustrates the number of r_p distributions of these WSAPs. The full WSAP sample shows a relatively flat distribution as a function of r_p , but the tidal sample drops off relatively quickly, with few tidal pairs out past $40 h_{70}^{-1} \text{ kpc}$.

The WSAPs allow us to observe more detailed interaction features in these systems. They are particularly valuable for tracing the early and intermediate stages of galaxy interactions, when gravitational torques and tidal perturbations begin to drive gas inflows toward the nuclei (J. E. Barnes & L. Hernquist 1992; P. F. Hopkins & E. Quataert 2010). The efficiency of such fueling depends on the orbital geometry, mass ratio, and gas content of the progenitors, producing diverse kinematic and morphological signatures (P. R. Capelo et al. 2017; T. J. Cox et al. 2008). Observational studies have shown that nuclear activity can arise in early-stage mergers and persist out to large separations (X. Liu et al. 2011b; M. Koss

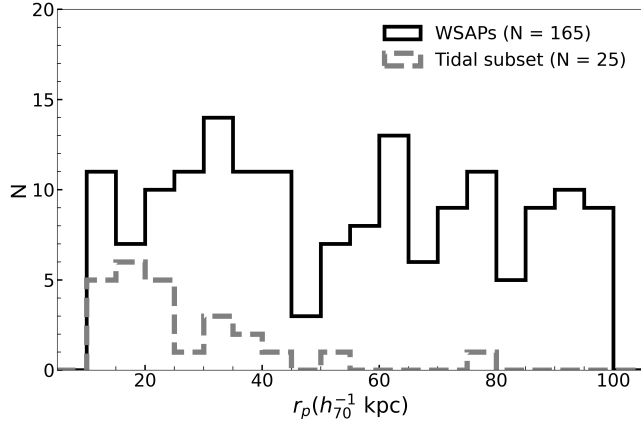


Figure 6. Distribution of projected distance (r_p) for our dual AGNs. The black solid step histogram represents the full WSAP sample ($N=165$), while the gray dashed step histogram corresponds to the tidal subset ($N=25$).

et al. 2012; A. De Rosa et al. 2023). Dual AGNs within <60 kpc often show gas inflow toward the nuclei, while systems beyond ~ 100 kpc may evolve without strong gas disturbances (A. De Rosa et al. 2023). Together, these results highlight the importance of investigating large-scale (10–100 kpc) dual AGNs, and our WSAP subsample offers an opportunity to probe the early co-evolution of SMBHs and their hosts, thereby enabling extrapolation to higher redshifts and enhancing our understanding of the fine details of merger-induced mass assembly.

3.3. Multiples, Extra Galaxies and/or AGN Candidates in the Pair Regions

Our sample includes five multiple AGNs (four triplets and one quadruplet), as presented in Figure 7 and listed in Table 3, where a system is included if at least one pair of objects satisfies the projected distance/ LOS velocity difference criterion outlined in Section 2.2. Some are optically selected (e.g., from SDSS DR16 or GSAC), while others are drawn from galaxy catalogs (PGC) or literature-based AGN compilations.

The projected distances among the nuclei in these systems range from 40 to $120 h_{70}^{-1}$ kpc. For instance, the closest members in J1332+0717 and J1511+1032 are separated by $\sim 40\text{--}50 h_{70}^{-1}$ kpc, while the most wide separation pairs exceed $90\text{--}100 h_{70}^{-1}$ kpc. In the quadruplet J2047+0024, the distances span from $\sim 49 h_{70}^{-1}$ kpc to more than $110 h_{70}^{-1}$ kpc. Notably, no sub-10 kpc multiple systems are present in our sample, underscoring the extreme rarity of compact triple or quadruple AGNs at low redshifts. DESI-LS images reveal disturbed host morphologies and possible tidal-like distortions in J1511+1032, consistent with interaction signa-

tures. However, other systems lack obvious tidal features.

During the visual inspection of our sample, we found several additional galaxies and/or AGN candidates located in the same regions as the pairs or multiplets. Based on the criteria laid out in Section 2.2, we identified 14 three-object, 8 four-object, 2 five-object, one six-object, one eight-object, and one nine-object systems. In this process, we also identified one additional LINER not included within the MQC. The basic data for a subset of these additional galaxy multiplets are listed in Table 4, along with their classifications obtained from SIMBAD (provided in the “Class” column). These AGN candidates are worthy of further observational confirmation, and the entire system merits in-depth study at multiple wavelengths.

4. DISCUSSION

We performed a systematic search of 103,216 AGNs at low redshifts ($z < 0.5$) in the MQC and identified 178 new multiple AGN systems, comprising 173 dual AGNs, 4 triple AGNs, and 1 quadruple AGN. In the MQC, dual AGNs constitute $\sim 0.34\%$ of the sample, while triple and quadruple AGNs account for $\sim 0.016\%$. For comparison, X. Liu et al. (2011b) analyzed 138,070 AGNs in the redshift range $0.02 < z < 0.33$ and reported 1,286 multiple AGN systems, including 1,244 dual AGNs, 39 triple AGNs, 2 quadruple AGNs, and 1 quintuple AGN, corresponding to fractions of $\sim 1.8\%$ and $\sim 0.09\%$ for dual and triple nucleus systems, respectively. The fraction of multiple AGNs reported by X. Liu et al. (2011b) is significantly higher than that found in the MQC sample. This discrepancy likely reflects the inhomogeneous nature of the MQC and differences in sample composition, most notably in the fraction of narrow-line AGNs (NLAGNs-NLQSOs), which constitute $\sim 61\%$ in the MQC compared to 94% in X. Liu et al. (2011b) sample. In addition, there is a marked concentration of systems at $z < 0.25$. Cosmological simulations predict that the fraction of dual AGNs should increase with redshift and peak around cosmic noon (Y. Chen et al. 2020; A. Foord et al. 2024), suggesting that the observed low-redshift concentration is primarily driven by selection effects inherent to the MQC. However, our sample has enhanced coverage at higher redshifts with 25.4% of pairs at $z > 0.16$ compared to only 1.9% in X. Liu et al. (2011b). While the MQC is an inhomogeneous parent sample, we do recover a significant number of higher redshift systems relative to prior samples.

Second, the dual AGNs are broadly uniformly distributed within the projected distance range of $0\text{--}100 h_{70}^{-1}$ kpc, and the tidal subsample is predominantly

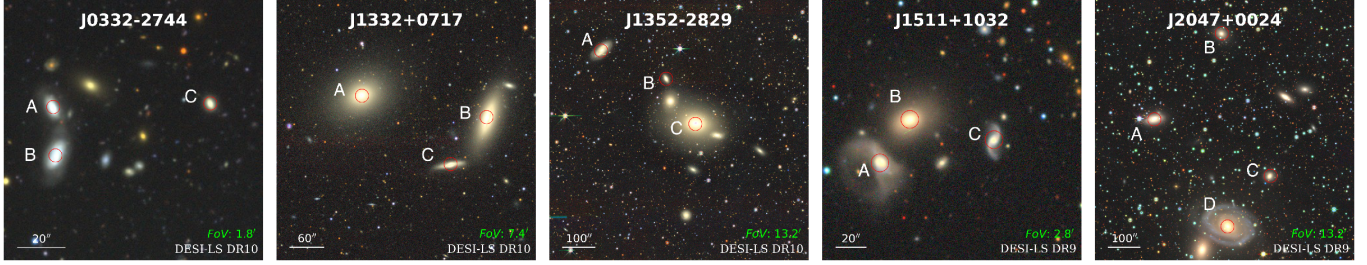


Figure 7. DESI-LS grz(i)-bands cutouts of five multi-AGN systems in our sample: four triple AGNs and one quadruple AGN. The components are labeled as A–D in each field.

Table 3. Basic parameters of the multi-AGN systems.

System	No.	RA (J2000)	DEC (J2000)	Class	Redshift	r_p (h_{70}^{-1} kpc)	Cite
J0332–2744	A:	53.124506	–27.740284	AX	0.076	28.36916	GSAC
	B:	53.104588	–27.734287	A	0.076	96.60849	GSAC
	C:	53.124941	–27.734830	AX	0.076	93.50298	GSAC
J1332+0717	A:	203.134409	7.294156	A	0.023	48.04549	PGC
	B:	203.116300	7.316590	NR	0.023	102.55542	PGC
	C:	203.177200	7.327290	AR	0.023	90.01932	PGC
J1352–2829	A:	208.312600	–28.427610	NX	0.015	65.55664	PGC
	B:	208.250722	–28.451806	NX	0.017	52.92251	PGC
	C:	208.222200	–28.489320	AX	0.016	110.77492	PGC
J1511+1032	A:	227.785414	10.537003	NR	0.07	43.55189	PGC
	B:	227.780110	10.544547	A	0.069	71.37602	PGC
	C:	227.764846	10.540903	A	0.067	95.18574	DR16
J2047+0024	A:	311.892100	0.411622	NX	0.012	81.53752	0478
	B:	311.834900	0.483990	N	0.014	112.69869	PGC
	C:	311.793786	0.363305	ARX	0.012	49.02998	PGC
	D:	311.829437	0.320811	A	0.014	97.52666	PGC

NOTE—Basic parameters of the five multiple AGN systems. The “Type” column gives the classifications provided in the MQC. The r_p column lists the projected distance between the paired components (e.g., A–B, B–C, etc.). The entry “0478” in the cite column is a reference to Milliquas, see its link provided in Table 1.

concentrated at $5\text{--}20 h_{70}^{-1}$ kpc. This is consistent with the statistics of [M. Koss et al. \(2012\)](#), who found that among 167 dual AGNs at $z < 0.05$ the majority lie within < 30 kpc with 50% (8/16) located at < 15 kpc. In addition, certain bins of the projected distance distribution (e.g., $45 \leq r_p \leq 50 h_{70}^{-1}$ kpc) contain relatively few systems. The apparent deficit of systems at small separations ($r_p \leq 5 h_{70}^{-1}$ kpc) is likely due to the angular resolution limits of major spectroscopic surveys. As shown in [Figure 9](#), the angular separation for $r_p < 5, h_{70}^{-1}$ kpc decreases with increasing redshift within $0 < z < 0.5$, reaching about $3''$ at $z \approx 0.09$, comparable to the SDSS

fiber size (DESI $\sim 1.5''$). Therefore, close dual nuclei are likely to be missed ([X. Liu et al. 2011b](#); [H. Fu et al. 2011a](#); [J. M. Comerford et al. 2012](#)), or source confused due to fiber spillover effects ([B. Husemann et al. 2018](#); [R. W. Pfeifle et al. 2023](#)) or extended narrow line regions (e.g., [H. Fu et al. 2012b, 2018](#); [W. C. Keel et al. 2019](#)).

The tidal subsamples reveal further insights. Those systems with large separations rarely exhibit tidal features, with only one case found at $> 55 h_{70}^{-1}$ kpc. As the projected distances decrease, the number of tidal systems rises markedly, peaking at 13 cases at $5\text{--}20 h_{70}^{-1}$ kpc. In the distribution of LOS velocity differences

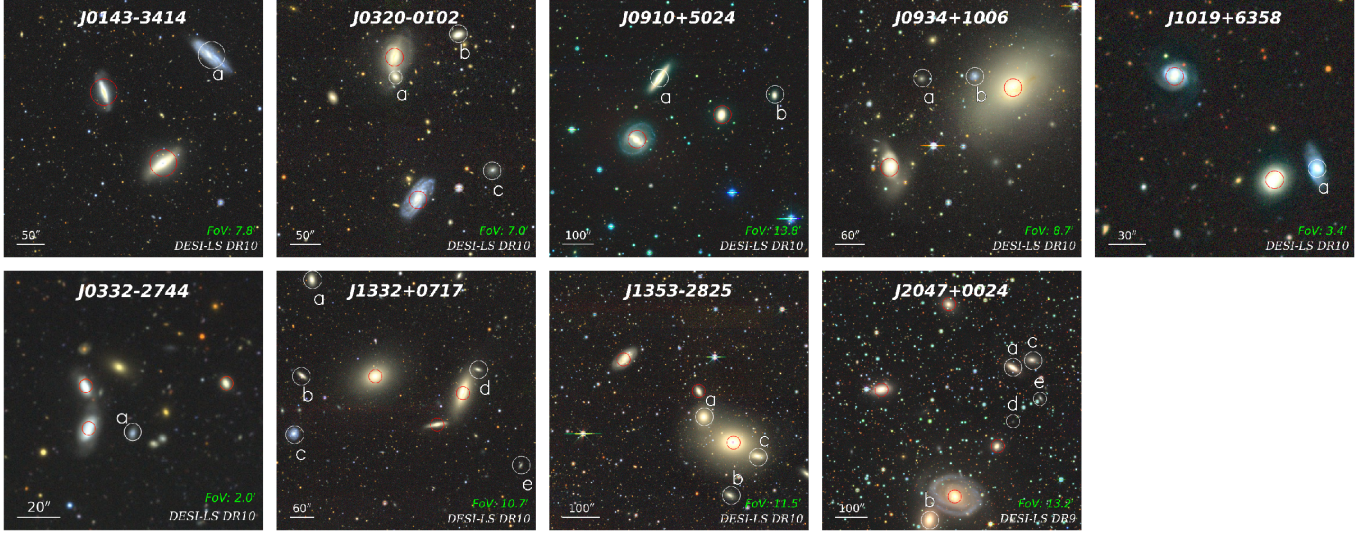


Figure 8. DESI-LS grz(i)-bands images of five pairs, three triplets, and a quadruplet with extra galaxies and/or AGN candidates. Red circles indicate the locations of AGNs. The numbered extra galaxies and/or AGN candidates are in white circles. North is up and east is to the left. The FOV of each image is labeled at the bottom right corner of the image.

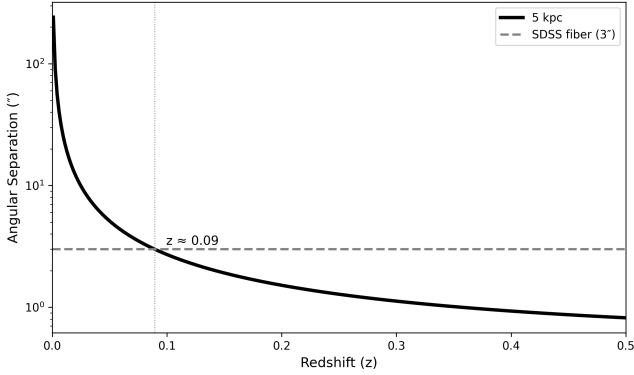


Figure 9. Angular separation as a function of redshift corresponding to a projected distance of $5 h_{70}^{-1}$ kpc. The blue dashed line indicates the SDSS fiber diameter of $3''$.

($|\Delta v|$), the number of dual AGNs declines with increasing $|\Delta v|$, and nearly all systems showing tidal features are confined to $|\Delta v| < 300 \text{ km s}^{-1}$, consistent with the statistical trend reported by X. Liu et al. (2011b). These results collectively suggest that the tidal features become less common in wide separation systems, consistent with the predictions from the IllustrisTNG simulations, in which close pairs ($r < 25$ kpc) have almost universally experienced recent pericentric passages and are expected to merge on short timescales (≤ 1 Gyr; (D. R. Patton et al. 2024)), whereas wider pairs are more often long-lived or non-merging systems with weak or absent tidal signatures. This indicates that larger physical distances may not favor the development or survival of tidal disturbances, possibly because (1) wide separation pairs are still in early merger stages where tidal features have not yet developed; (2) some systems have undergone

close passages but with orbital or mass configurations not conducive to strong tidal signatures; or (3) galaxies have moved away from pericenter, and earlier tidal features have already dissipated. It is also important to emphasize that the projected pair separation serves as a proxy for the merger stage, but in general it is a degenerate property; different merger stages/orbital configurations can show similar or the same projected separation (e.g., J. E. Barnes & L. Hernquist 1996; T. J. Cox et al. 2008; P. R. Capelo et al. 2015; R. W. Pfeifle et al. 2025). In addition, the number of dual AGNs drops when $|\Delta v| \gtrsim 300 \text{ km s}^{-1}$, consistent with the trend seen in X. Liu et al. (2011b) sample, as mentioned in Section 3.1.

Beyond dual AGNs, we identified four triplets and one quadruplet system. These findings extend previous studies of multiple-AGN systems. Earlier works have reported a single bona fide, compact (sub-10 kpc) triple AGN system (R. W. Pfeifle et al. 2019; X. Liu et al. 2019), and confirmed Hickson Compact Group 16 as a triple AGN with larger separations (X. Liu et al. 2011b; M. J. L. Turner et al. 2001; M. Koss et al. 2012). On galaxy-group scales, multiwavelength observations of compact groups (A. De Rosa et al. 2015) have provided valuable insights into the mechanisms that trigger nuclear activity and star formation. Compared to these systems, our multiple-AGN samples exhibit separations of tens of kiloparsecs without pronounced tidal features, yet they represent a valuable intermediate-scale population for tracing the full evolutionary sequence of multiple-AGN activity and for probing the mechanisms that trigger nuclear accretion at different merger stages.

Table 4. Catalog of Extra galaxies or AGNs (or Candidates) in the pair regions.

System	Obj.name	RA	Dec	z	$\Delta\theta$	r_p	$ \Delta v $	Class
(1)	(2)	(J2000)	(J2000)	(5)	($''$)	(h_{70}^{-1} kpc)	(km s^{-1})	(9)
J0143-3414	ⒶIC 1722	25.76242	-34.18733	0.01384	202.89	52.184	371.89	LSBG
J0320-0102	ⒶLEDA 12538	50.18886	-1.05395	0.02079	37.51	15.783	179.22	Galaxy
	ⒷZ 390-67	50.16065	-1.03503	0.02101	112.52	47.839	114.57	EmG
	ⒸLEDA 1126869	50.14511	-1.09587	0.02139	133.33	56.433	141.02	EmG
J0910+5024	ⒶNGC 2769	137.63393	50.43325	0.01607	193.81	63.411	274.46	LINER
	ⒷNGC 2762	137.47723	50.41826	0.01564	179.25	57.111	233.26	AGN Candidate
J0934+1006	ⒶSDSS J093358.56+100928.3	143.49403	10.15787	0.01195	186.36	41.168	347.65	AGN Candidate
	ⒷNGC 2912	143.46364	10.15937	0.01106	81.82	18.074	81.61	AGN Candidate
J1019+6358	ⒶMCG+11-13-017	154.78098	63.96993	0.04152	35.27	28.919	0.58	Galaxy
J0332-2744	ⒶEIS-DEEP CDFS-1 J 1 247	53.11808	-27.74062	0.0726	21.05	29.093	949.46	EmG
J1332+0717	ⒶZ 45-12	203.22101	7.39347	0.02251	285.00	129.611	255.15	GinGroup
	ⒷZ 45-11	203.22781	7.32769	0.02375	180.71	85.269	108.44	Galaxy
	ⒸNGC 5212	203.23345	7.28786	0.02375	245.94	116.048	553.54	GinGroup
	ⒹSDSS J133225.48+071954.6	203.10618	7.33184	0.02335	65.72	30.971	8.79	Galaxy
	ⒺSDSS J133218.37+071557.9	203.07646	7.26614	0.02161	230.70	100.853	517.94	AGN Candidate
J1353+2825	ⒶNGC 5330	208.24666	-28.47072	0.01630	69.32	22.997	101.89	GinGroup
	Ⓑ2MASX J13525393-2831421	208.22473	-28.52837	0.01708	140.98	45.351	380.83	GinCl
	ⒸLEDA 3094716	208.20170	-28.49947	0.01528	74.35	23.158	150.68	EmG
J2047+0024	ⒶNGC 6959	311.78017	0.43017	0.01222	245.67	61.412	53.34	Galaxy
	ⒷNGC 6964	311.85126	0.30083	0.01265	106.52	27.550	402.63	AGN Candidate
	ⒸLEDA 162626	311.76379	0.43679	0.01257	285.74	72.464	50.37	AGN Candidate
	ⒹSDSS J204707.21+002302.9	311.78001	0.38418	0.01284	90.03	22.832	130.35	AGN Candidate
	ⒺLEDA 1165076	311.75643	0.40443	0.01400	199.99	50.718	460.55	AGN Candidate

NOTE—Columns: (1)-(5) System Name, Name of extra galaxies and/or AGN Candidates, Coordinates (deg), Redshift of extra galaxies or AGNs (or Candidates); (6)-(8) Angular separation, projected distance, and LOS velocity difference from the nearest AGN of the system; (9) Source classifications as retrieved from the SIMBAD database^a. The abbreviations used are: LSBG for Low Surface Brightness Galaxy, EmG for Emission-line Galaxy, GinGroup for Galaxy towards a Group of Galaxies, and GinCl for Galaxy towards a Cluster of Galaxies.

(This entire table is available in machine-readable form.)

^a<https://simbad.cds.unistra.fr/simbad/>

Confirmed multiples remain exceedingly rare (M. J. L. Turner et al. 2001; M. Koss et al. 2012; X. Liu et al. 2011a; K. Schawinski et al. 2011; X. Liu et al. 2019). Yet, their existence is also consistent with the hierarchical merging scenario, in which dense environments provide ample cold gas to fuel SMBH accretion (A. K. Bhowmick et al. 2020; J. F. Hennawi et al. 2006). Moreover, interactions among multiple SMBHs in these systems may accelerate SMBH growth and eventual coalescence (C. Hoffman et al. 2023). Therefore, multiple-AGN systems serve as ideal laboratories for understanding the co-evolution of SMBHs and their host galaxies

(M. Fukugita et al. 2004; P. J. Green et al. 2011; K. Husband et al. 2013).

We also found some extra galaxies and/or AGN candidates by visual inspection. Detailed observations of these systems may reveal further cases of AGNs multiplets, as well as more information on the fueling and feedback processes of multi-AGNs in galaxy merger groups.

5. CONCLUSION

In this work, we use the Million Quasar Catalog (MQC, version 8.0; E. W. Flesch 2023)⁶ as the parent catalog. From it, we construct a low-redshift ($z < 0.5$) sample of dual AGNs and multiplets. Based on this sample, we perform statistical analyses. Our main conclusions are summarized as follows:

- We applied stringent selection criteria, specifically (1) a projected separation of $r_p < 100 h_{70}^{-1}$ kpc, and (2) a line-of-sight velocity difference of $|\Delta v| < 600 \text{ km s}^{-1}$. Based on these criteria, we ultimately identified 173 dual AGNs, 4 AGN triplets, and 1 AGN quadruplet. Visual inspection of optical images from the DESI–LS were performed for each pair, revealing that approximately 16% of the dual AGNs exhibit tidal features.
- In our sample, AGN-NLAGNs (35.3%) and NLAGN-NLAGNs (35.8%) constitute the majority, indicating that narrow-line AGNs dominate in low-redshift dual AGN systems. The dual AGNs are generally uniformly distributed in projected distances between $0\text{--}100 h_{70}^{-1}$ kpc. The distribution of the tidal sample peaks sharply at $r_p \approx 5\text{--}20 h_{70}^{-1}$ kpc, which accounts for 13 pairs. The frequency then falls rapidly with increasing separation, with only a single pair located beyond $55 h_{70}^{-1}$ kpc. Beyond $80 h_{70}^{-1}$ kpc, tidal pairs are entirely absent.
- The redshift distribution of dual AGNs shows that within the range of $0.02 < z < 0.33$, the fraction of dual and multiple AGNs identified in the MQC is significantly lower than that reported by X. Liu et al. (2011b) for their sample.
- Regarding the LOS velocity difference ($|\Delta v|$), the number of dual AGNs decreases with increasing $|\Delta v|$, with only a few systems approaching the upper limit of 600 km s^{-1} . Systems exhibiting tidal features are predominantly found at $|\Delta v| < 300 \text{ km s}^{-1}$, indicating that larger velocity differences generally correspond to greater physical separa-

tions, which are less conducive to the formation or persistence of prominent tidal structures.

- We discuss a close system, J1053+4710 ($r_p < 5 h_{70}^{-1}$ kpc), which shows a possible dual-nucleus morphology but the spectroscopic evidence is not sufficient to confirm a dual AGN nature. In addition, 165 wide separation pairs ($r_p > 10 h_{70}^{-1}$ kpc) were identified, including 25 with clear tidal features, enriching the known population of large-scale interacting dual AGNs.
- We found some extra galaxies and/or AGN candidates in the same regions of some dual AGNs or multiplets, and some objects form interacting systems with the dual AGNs or multiplets. In total, we found 2 three-object, 3 four-object, 1 five-object, 1 six-object, 1 eight-object and 1 nine-object interacting systems.

The MQC is inherently inhomogeneous, being compiled from diverse observational methods and archival datasets. Consequently, systematic biases and incompleteness may remain across different sky regions or redshift ranges, and the statistical results presented here should therefore be interpreted with caution. Nevertheless, with the advent of upcoming large-scale spectroscopic and photometric surveys such as DESI, 4MOST, and CSST, the number of confirmed dual and multiple AGNs is expected to increase substantially. These future surveys will enable the construction of a more complete and homogeneous sample, offering unprecedented opportunities to investigate the demographics, triggering mechanisms, and co-evolution of AGNs and their host galaxies across cosmic time.

ACKNOWLEDGMENTS

This work has been supported by the Chinese National Natural Science Foundation grants 12333001, and by the National Key R&D Program of China (2021YFA0718500, 2025YFA1614101). We would like to express our gratitude to Yue Han, for her unwavering support, and encouragement throughout the course of this research. Special thanks to Meicun Hou for her assistance during the research process.

APPENDIX

⁶ <https://heasarc.gsfc.nasa.gov/W3Browse/all/milliquas.html>

DUAL AGN SAMPLE MOSAIC

Figure 1 presents the mosaic of the dual AGN system identified in this work. Each panel shows the g , r , and $z(i)$ -band composite images from the DESI Legacy Surveys DR10, together with their corresponding model and residual images provided by the survey. These visualizations illustrate the morphological features and the model-fitting performance across our sample. It should be noted that some pairs lie at declinations lower than -30° , where DESI imaging is not available, therefore, the displayed sample is not complete.

For the pairs J0114–5523 and J1419+5244, the MQC lists positions for two components, but only one component is apparent in the LS images at the expected locations. According to the MQC documentation⁷, both objects are classified as type ‘N’, a broad category that includes narrow-line AGNs, type-II Seyferts, and host-dominated systems, among other unquantified residue of legacy narrow-emission-line classes. This broad classification, together with potential astrometric uncertainties and/or a counterpart below the LS detection limit, may contribute to the apparent absence of the second component in the images.

⁷ <http://www.quasars.org/Milliquas-ReadMe.txt>

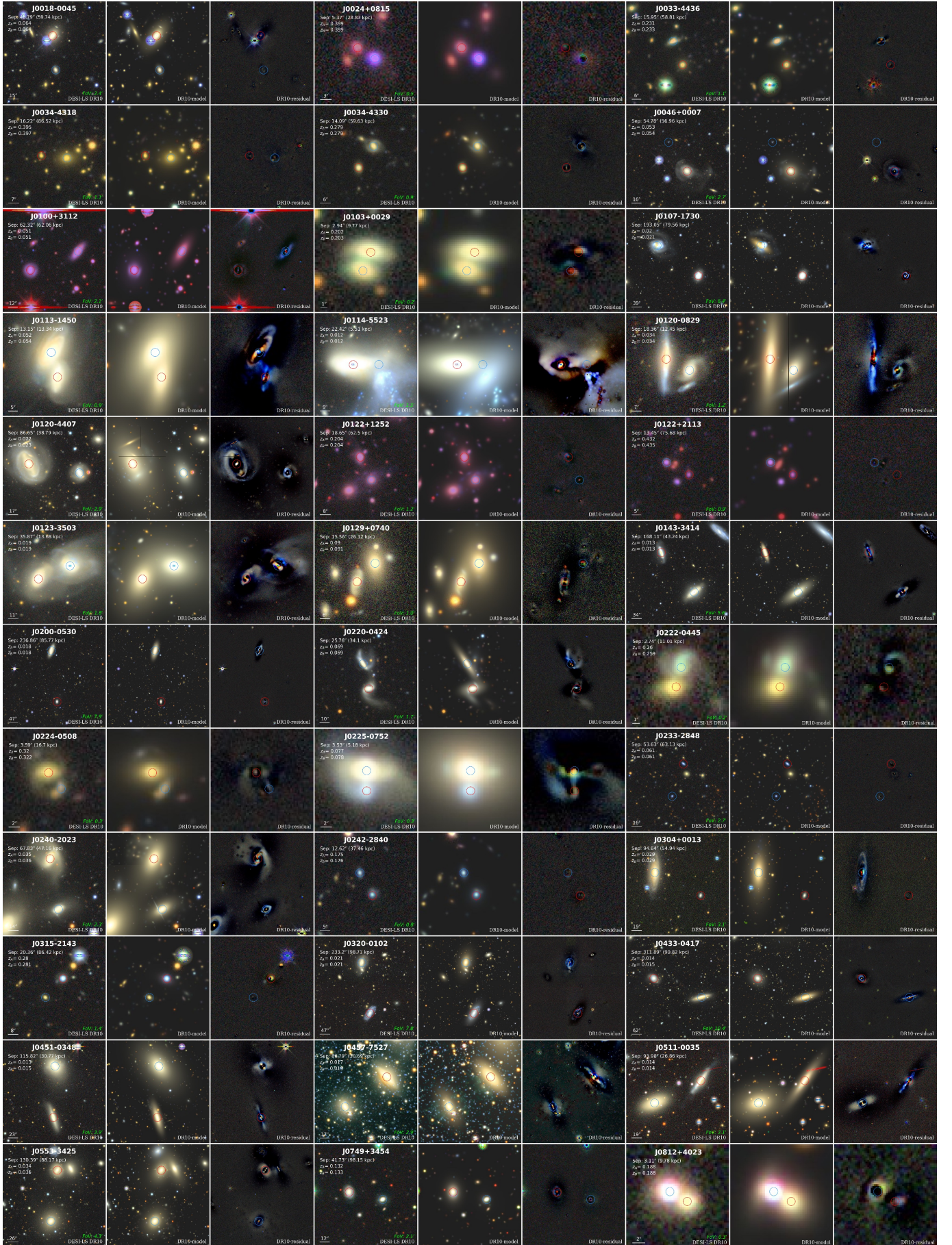


Figure 1. Mosaic of dual AGN systems. Each triplet of images shows the $grz(i)$ -band composite, the corresponding model, and the residual map from DESI Legacy Surveys DR10. The pinkish appearance in some images is likely due to incomplete band coverage.

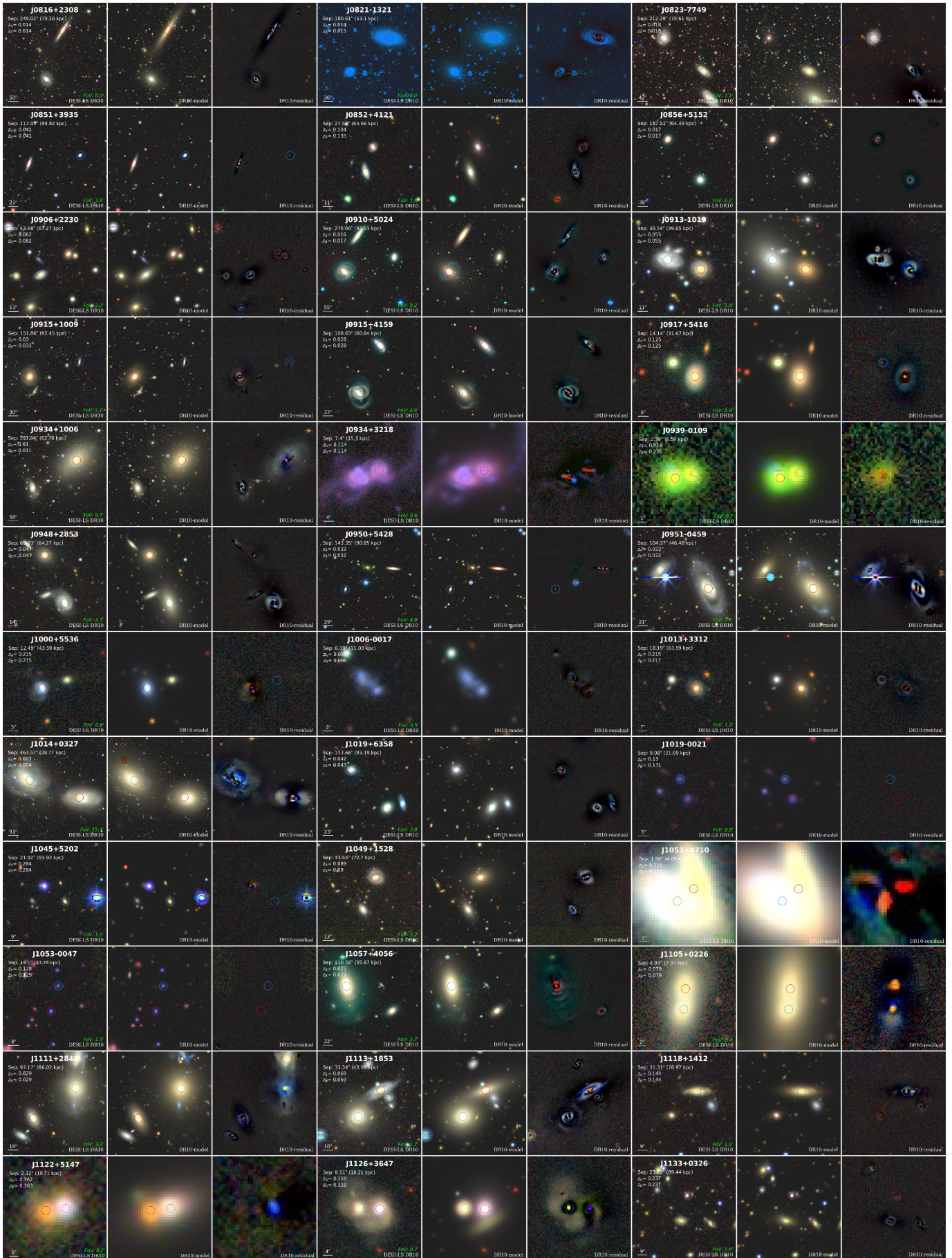


Figure 1. - continued

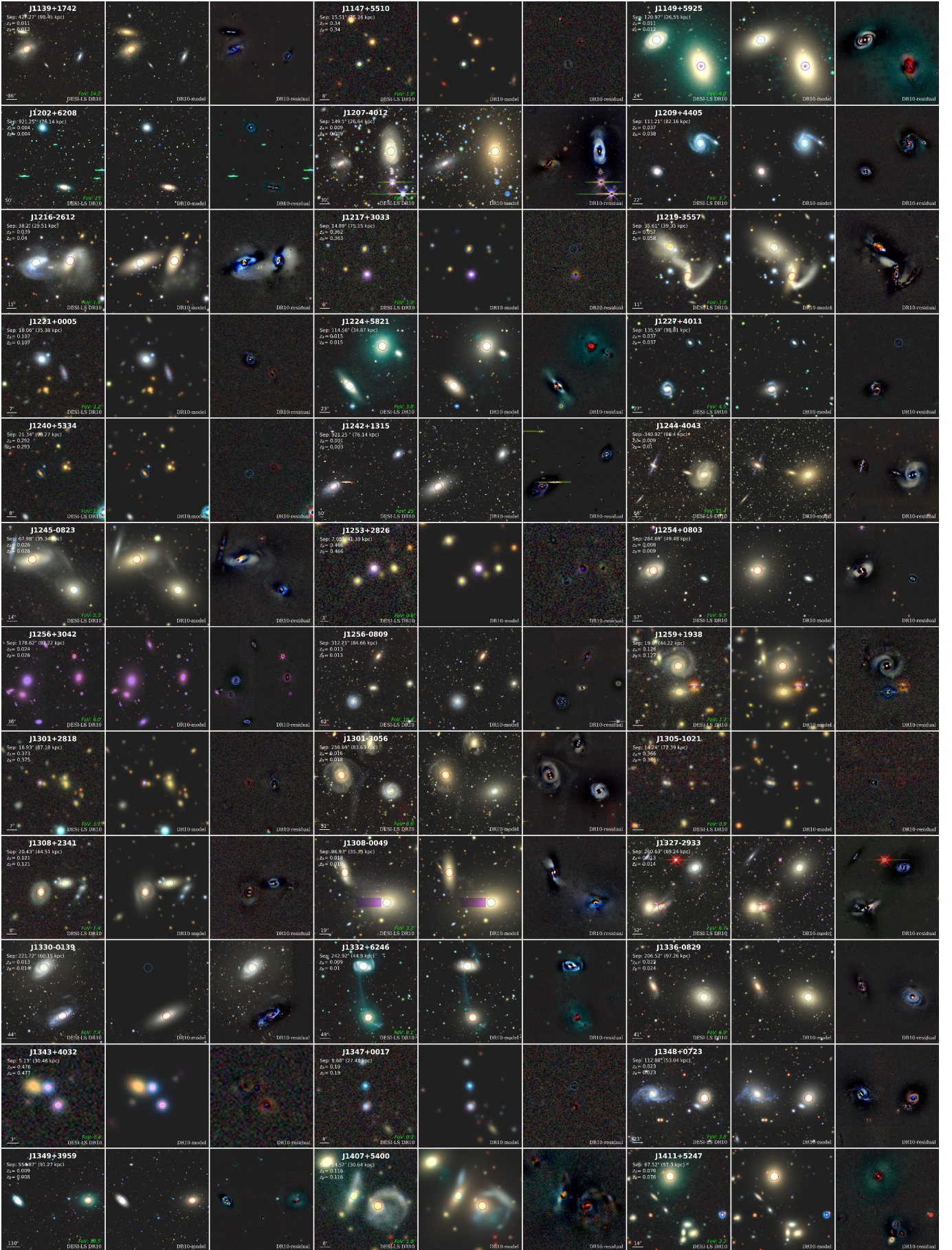


Figure 1. - continued



Figure 1. - continued

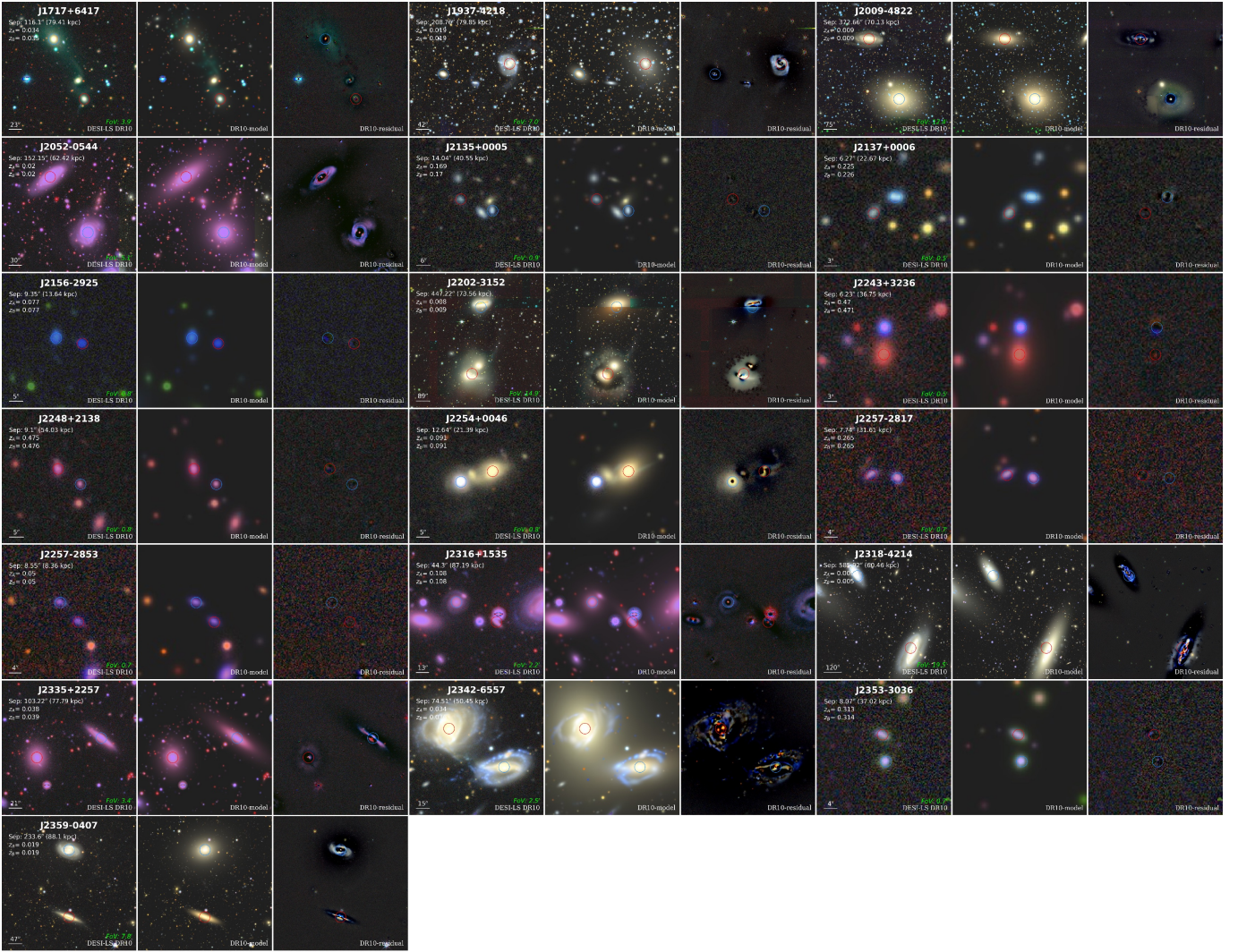


Figure 1. - continued

REFERENCES

- Amaro-Seoane, P., Andrews, J., Arca Sedda, M., et al. 2023, *Living Reviews in Relativity*, 26, doi: [10.1007/s41114-022-00041-y](https://doi.org/10.1007/s41114-022-00041-y)
- Armitage, P. J., & Natarajan, P. 2002, *ApJL*, 567, L9, doi: [10.1086/339770](https://doi.org/10.1086/339770)
- Arzoumanian, Z., Baker, P. T., Blumer, H., et al. 2020, *ApJL*, 905, L34, doi: [10.3847/2041-8213/abd401](https://doi.org/10.3847/2041-8213/abd401)
- Ballo, L., Braito, V., Ceca, R. D., et al. 2004, *ApJ*, 600, 634, doi: [10.1086/379887](https://doi.org/10.1086/379887)
- Barnes, J. E., & Hernquist, L. 1992, *ARA&A*, 30, 705, doi: [10.1146/annurev.aa.30.090192.003421](https://doi.org/10.1146/annurev.aa.30.090192.003421)
- Barnes, J. E., & Hernquist, L. 1996, *ApJ*, 471, 115, doi: [10.1086/177957](https://doi.org/10.1086/177957)
- Barton, E. J., Geller, M. J., & Kenyon, S. J. 2000, *ApJ*, 530, 660, doi: [10.1086/308392](https://doi.org/10.1086/308392)
- Begelman, M. C., Blandford, R. D., & Rees, M. J. 1980, *Nature*, 287, 307, doi: [10.1038/287307a0](https://doi.org/10.1038/287307a0)
- Bhowmick, A. K., Di Matteo, T., & Myers, A. D. 2020, *MNRAS*, 492, 5620, doi: [10.1093/mnras/staa172](https://doi.org/10.1093/mnras/staa172)
- Bianchi, S., Chiaberge, M., Piconcelli, E., Guainazzi, M., & Matt, G. 2008, *MNRAS*, 386, 105, doi: [10.1111/j.1365-2966.2008.13078.x](https://doi.org/10.1111/j.1365-2966.2008.13078.x)
- Blecha, L., Loeb, A., & Narayan, R. 2013, *MNRAS*, 429, 2594, doi: [10.1093/mnras/sts533](https://doi.org/10.1093/mnras/sts533)
- Blumenthal, K. A., & Barnes, J. E. 2018, *MNRAS*, 479, 3952, doi: [10.1093/mnras/sty1605](https://doi.org/10.1093/mnras/sty1605)
- Capelo, P. R., Dotti, M., Volonteri, M., et al. 2017, *MNRAS*, 469, 4437, doi: [10.1093/mnras/stx1067](https://doi.org/10.1093/mnras/stx1067)
- Capelo, P. R., Volonteri, M., Dotti, M., et al. 2015, *MNRAS*, 447, 2123, doi: [10.1093/mnras/stu2500](https://doi.org/10.1093/mnras/stu2500)
- Chen, Y., Yu, Q., & Lu, Y. 2020, *ApJ*, 897, 86, doi: [10.3847/1538-4357/ab9594](https://doi.org/10.3847/1538-4357/ab9594)
- Chen, Y.-C., Liu, X., Lazio, J., et al. 2023, *ApJ*, 958, 29, doi: [10.3847/1538-4357/ad00b3](https://doi.org/10.3847/1538-4357/ad00b3)
- Comerford, J. M., Gerke, B. F., Stern, D., et al. 2012, *ApJ*, 753, 42, doi: [10.1088/0004-637X/753/1/42](https://doi.org/10.1088/0004-637X/753/1/42)
- Comerford, J. M., Griffith, R. L., Gerke, B. F., et al. 2009b, *ApJ*, 702, L82, doi: [10.1088/0004-637X/702/1/L82](https://doi.org/10.1088/0004-637X/702/1/L82)
- Conselice, C. J. 2003, *ApJS*, 147, 1, doi: [10.1086/375001](https://doi.org/10.1086/375001)
- Conselice, C. J. 2014, *ARA&A*, 52, 291, doi: [10.1146/annurev-astro-081913-040037](https://doi.org/10.1146/annurev-astro-081913-040037)
- Cox, T. J., Jonsson, P., Somerville, R. S., Primack, J. R., & Dekel, A. 2008, *MNRAS*, 384, 386, doi: [10.1111/j.1365-2966.2007.12730.x](https://doi.org/10.1111/j.1365-2966.2007.12730.x)
- Darg, D. W., Kaviraj, S., Lintott, C. J., et al. 2010, *MNRAS*, 401, 1043, doi: [10.1111/j.1365-2966.2009.15686.x](https://doi.org/10.1111/j.1365-2966.2009.15686.x)
- De Rosa, A., Bianchi, S., Bogdanović, T., et al. 2015, *MNRAS*, 453, 214, doi: [10.1093/mnras/stv1623](https://doi.org/10.1093/mnras/stv1623)
- De Rosa, A., Vignali, C., Severgnini, P., et al. 2023, *MNRAS*, 519, 5149, doi: [10.1093/mnras/stac3664](https://doi.org/10.1093/mnras/stac3664)
- Dey, A., Schlegel, D. J., Lang, D., et al. 2019, *AJ*, 157, 168, doi: [10.3847/1538-3881/ab089d](https://doi.org/10.3847/1538-3881/ab089d)
- Di Matteo, T., Springel, V., & Hernquist, L. 2005, *Nature*, 433, 604, doi: [10.1038/nature03335](https://doi.org/10.1038/nature03335)
- Dotti, M., Colpi, M., Haardt, F., & Mayer, L. 2007, *MNRAS*, 379, 956, doi: [10.1111/j.1365-2966.2007.12010.x](https://doi.org/10.1111/j.1365-2966.2007.12010.x)
- Dotti, M., Sesana, A., & Decarli, R. 2012, *AdAst*, 2012, 940568, doi: [10.1155/2012/940568](https://doi.org/10.1155/2012/940568)
- Dux, F., Lemon, C., Courbin, F., et al. 2024, *A&A*, 682, A47, doi: [10.1051/0004-6361/202347598](https://doi.org/10.1051/0004-6361/202347598)
- Ellison, S. L., Patton, D. R., Simard, L., & McConnachie, A. W. 2008, *AJ*, 135, 1877, doi: [10.1088/0004-6256/135/5/1877](https://doi.org/10.1088/0004-6256/135/5/1877)
- EPTA Collaboration, InPTA Collaboration, Antoniadis, J., et al. 2024, *A&A*, 685, A94, doi: [10.1051/0004-6361/202347433](https://doi.org/10.1051/0004-6361/202347433)
- Flesch, E., & Hardcastle, M. J. 2004, *A&A*, 427, 387, doi: [10.1051/0004-6361:20041076](https://doi.org/10.1051/0004-6361:20041076)
- Flesch, E. W. 2023, *The Open Journal of Astrophysics*, 6, 49, doi: [10.21105/astro.2308.01505](https://doi.org/10.21105/astro.2308.01505)
- Flesch, E. W. 2024, *The Open Journal of Astrophysics*, 7, 6, doi: [10.21105/astro.2308.01507](https://doi.org/10.21105/astro.2308.01507)
- Foord, A., Cappelluti, N., Liu, T., et al. 2024, *Universe*, 10, 237, doi: [10.3390/universe10060237](https://doi.org/10.3390/universe10060237)
- Fu, H., Myers, A. D., Djorgovski, S. G., & Yan, L. 2011a, *ApJ*, 733, 103, doi: [10.1088/0004-637X/733/2/103](https://doi.org/10.1088/0004-637X/733/2/103)
- Fu, H., Yan, L., Myers, A. D., et al. 2012a, *ApJ*, 745, 67, doi: [10.1088/0004-637X/745/1/67](https://doi.org/10.1088/0004-637X/745/1/67)
- Fu, H., Yan, L., Myers, A. D., et al. 2012b, *ApJ*, 745, 67, doi: [10.1088/0004-637X/745/1/67](https://doi.org/10.1088/0004-637X/745/1/67)
- Fu, H., Zhang, Z.-Y., Assef, R. J., et al. 2011b, *ApJL*, 740, L44, doi: [10.1088/2041-8205/740/2/L44](https://doi.org/10.1088/2041-8205/740/2/L44)
- Fu, H., Steffen, J. L., Gross, A. C., et al. 2018, *ApJ*, 856, 93, doi: [10.3847/1538-4357/aab364](https://doi.org/10.3847/1538-4357/aab364)
- Fukugita, M., Nakamura, O., Schneider, D. P., Doi, M., & Kashikawa, N. 2004, *ApJL*, 603, L65, doi: [10.1086/383222](https://doi.org/10.1086/383222)
- Green, P. J., Myers, A. D., Barkhouse, W. A., et al. 2011, *ApJ*, 743, 81, doi: [10.1088/0004-637X/743/1/81](https://doi.org/10.1088/0004-637X/743/1/81)
- Haehnelt, M. G. 1994, *MNRAS*, 269, 199, doi: [10.1093/mnras/269.1.199](https://doi.org/10.1093/mnras/269.1.199)
- Hawking, S. W., & Israel, W. 1987, *Three hundred years of gravitation* (Cambridge Univ. Press)
- Hennawi, J. F., Myers, A. D., Shen, Y., et al. 2010, *ApJ*, 719, 1672, doi: [10.1088/0004-637X/719/2/1672](https://doi.org/10.1088/0004-637X/719/2/1672)
- Hennawi, J. F., Strauss, M. A., Oguri, M., et al. 2006, *AJ*, 131, 1, doi: [10.1086/498235](https://doi.org/10.1086/498235)

- Hoffman, C., Chen, N., Di Matteo, T., et al. 2023, MNRAS, 524, 1987, doi: [10.1093/mnras/stad1929](https://doi.org/10.1093/mnras/stad1929)
- Hogg, D. W. 2000, Distance measures in cosmology, <https://arxiv.org/abs/astro-ph/9905116>
- Holz, D. E., & Hughes, S. A. 2005, ApJ, 629, 15, doi: [10.1086/431341](https://doi.org/10.1086/431341)
- Hopkins, P. F., Hernquist, L., Cox, T. J., et al. 2006, ApJS, 163, 1, doi: [10.1086/499298](https://doi.org/10.1086/499298)
- Hopkins, P. F., Hernquist, L., Cox, T. J., & Kereš, D. 2008, ApJS, 175, 356, doi: [10.1086/524362](https://doi.org/10.1086/524362)
- Hopkins, P. F., & Quataert, E. 2010, MNRAS, 407, 1529, doi: [10.1111/j.1365-2966.2010.17064.x](https://doi.org/10.1111/j.1365-2966.2010.17064.x)
- Husband, K., Bremer, M. N., Stanway, E. R., et al. 2013, MNRAS, 432, 2869, doi: [10.1093/mnras/stt642](https://doi.org/10.1093/mnras/stt642)
- Husemann, B., Worseck, G., Arrigoni Battaia, F., & Shanks, T. 2018, A&A, 610, L7, doi: [10.1051/0004-6361/201732457](https://doi.org/10.1051/0004-6361/201732457)
- Inada, N., Oguri, M., Shin, M.-S., et al. 2012, AJ, 143, 119, doi: [10.1088/0004-6256/143/5/119](https://doi.org/10.1088/0004-6256/143/5/119)
- Iwasawa, K., Mazzarella, J. M., Surace, J. A., et al. 2011, A&A, 528, A137, doi: [10.1051/0004-6361/201015872](https://doi.org/10.1051/0004-6361/201015872)
- Kauffmann, G., & Haehnelt, M. 2000, MNRAS, 311, 576, doi: [10.1046/j.1365-8711.2000.03077.x](https://doi.org/10.1046/j.1365-8711.2000.03077.x)
- Keel, W. C., Bennert, V. N., Pancoast, A., et al. 2019, MNRAS, 483, 4847, doi: [10.1093/mnras/sty3332](https://doi.org/10.1093/mnras/sty3332)
- Komossa, S., Burwitz, V., Hasinger, G., et al. 2003, ApJ, 582, L15, doi: [10.1086/346145](https://doi.org/10.1086/346145)
- Kormendy, J. 2013, in IAU Symposium, Vol. 295, The Intriguing Life of Massive Galaxies, ed. D. Thomas, A. Pasquali, & I. Ferreras, 241–256, doi: [10.1017/S174392131300495X](https://doi.org/10.1017/S174392131300495X)
- Kormendy, J., & Richstone, D. 1995, ARA&A, 33, 581, doi: [10.1146/annurev.aa.33.090195.003053](https://doi.org/10.1146/annurev.aa.33.090195.003053)
- Koss, M., Mushotzky, R., Treister, E., et al. 2012, ApJL, 746, L22, doi: [10.1088/2041-8205/746/2/L22](https://doi.org/10.1088/2041-8205/746/2/L22)
- Koss, M., Mushotzky, R., Treister, E., et al. 2011, ApJL, 735, L42, doi: [10.1088/2041-8205/735/2/L42](https://doi.org/10.1088/2041-8205/735/2/L42)
- Koss, M. J., Glidden, A., Baloković, M., et al. 2016, ApJL, 824, L4, doi: [10.3847/2041-8205/824/1/L4](https://doi.org/10.3847/2041-8205/824/1/L4)
- Lemon, C. A., Auger, M. W., McMahan, R. G., & Ostrovski, F. 2018, MNRAS, 479, 5060, doi: [10.1093/mnras/sty911](https://doi.org/10.1093/mnras/sty911)
- Liu, X., Greene, J. E., Shen, Y., & Strauss, M. A. 2010a, ApJ, 715, L30, doi: [10.1088/2041-8205/715/1/L30](https://doi.org/10.1088/2041-8205/715/1/L30)
- Liu, X., Shen, Y., & Strauss, M. A. 2011a, ApJL, 736, L7, doi: [10.1088/2041-8205/736/1/L7](https://doi.org/10.1088/2041-8205/736/1/L7)
- Liu, X., Shen, Y., Strauss, M. A., & Greene, J. E. 2010, ApJ, 708, 427, doi: [10.1088/0004-637X/708/1/427](https://doi.org/10.1088/0004-637X/708/1/427)
- Liu, X., Shen, Y., Strauss, M. A., & Hao, L. 2011b, ApJ, 737, 101, doi: [10.1088/0004-637X/737/2/101](https://doi.org/10.1088/0004-637X/737/2/101)
- Liu, X., Hou, M., Li, Z., et al. 2019, ApJ, 887, 90, doi: [10.3847/1538-4357/ab54c3](https://doi.org/10.3847/1538-4357/ab54c3)
- Lotz, J. M., Jonsson, P., Cox, T. J., & Primack, J. R. 2008, MNRAS, 391, 1137, doi: [10.1111/j.1365-2966.2008.14004.x](https://doi.org/10.1111/j.1365-2966.2008.14004.x)
- Lotz, J. M., Jonsson, P., Cox, T. J., & Primack, J. R. 2008, MNRAS, 391, 1137, doi: [10.1111/j.1365-2966.2008.14004.x](https://doi.org/10.1111/j.1365-2966.2008.14004.x)
- Lotz, J. M., Jonsson, P., Cox, T. J., & Primack, J. R. 2010, MNRAS, 404, 575, doi: [10.1111/j.1365-2966.2010.16268.x](https://doi.org/10.1111/j.1365-2966.2010.16268.x)
- Lotz, J. M., Primack, J., & Madau, P. 2004, AJ, 128, 163, doi: [10.1086/421849](https://doi.org/10.1086/421849)
- Mihos, J. C., & Hernquist, L. 1996, ApJ, 464, 641, doi: [10.1086/177353](https://doi.org/10.1086/177353)
- Milosavljević, M., & Merritt, D. 2001, ApJ, 563, 34, doi: [10.1086/323830](https://doi.org/10.1086/323830)
- Myers, A. D., Brunner, R. J., Nichol, R. C., et al. 2007, ApJ, 658, 85, doi: [10.1086/511519](https://doi.org/10.1086/511519)
- Myers, A. D., Brunner, R. J., Richards, G. T., et al. 2006, ApJ, 638, 622, doi: [10.1086/499093](https://doi.org/10.1086/499093)
- Owen, F. N., O’Dea, C. P., Inoue, M., & Eilek, J. A. 1985, ApJ, 294, L85, doi: [10.1086/184514](https://doi.org/10.1086/184514)
- Patton, D. R., Faria, L., Hani, M. H., et al. 2024, MNRAS, 529, 1493, doi: [10.1093/mnras/stae608](https://doi.org/10.1093/mnras/stae608)
- Pfeifle, R. W., Rothberg, B., Weaver, K. A., et al. 2023, ApJ, 945, 167, doi: [10.3847/1538-4357/acbd45](https://doi.org/10.3847/1538-4357/acbd45)
- Pfeifle, R. W., Weaver, K. A., Secrest, N. J., Rothberg, B., & Patton, D. R. 2025, ApJS, 281, 25, doi: [10.3847/1538-4365/adf845](https://doi.org/10.3847/1538-4365/adf845)
- Pfeifle, R. W., Satyapal, S., Manzano-King, C., et al. 2019, ApJ, 883, 167, doi: [10.3847/1538-4357/ab3a9b](https://doi.org/10.3847/1538-4357/ab3a9b)
- Piconcelli, E., Vignali, C., Bianchi, S., et al. 2010, ApJ, 722, L147, doi: [10.1088/2041-8205/722/2/L147](https://doi.org/10.1088/2041-8205/722/2/L147)
- Reardon, D. J., Zic, A., Shannon, R. M., et al. 2023, ApJL, 951, L7, doi: [10.3847/2041-8213/acdd03](https://doi.org/10.3847/2041-8213/acdd03)
- Richstone, D., Ajhar, E. A., Bender, R., et al. 1998, Nature, 385, A14, doi: [10.48550/arXiv.astro-ph/9810378](https://doi.org/10.48550/arXiv.astro-ph/9810378)
- Rodriguez, C., Taylor, G. B., Zavala, R. T., et al. 2006, ApJ, 646, 49, doi: [10.1086/504825](https://doi.org/10.1086/504825)
- Rosa, A. D., Vignali, C., Bogdanović, T., et al. 2019, NewAR, 86, 101525, doi: [10.1016/j.newar.2020.101525](https://doi.org/10.1016/j.newar.2020.101525)
- Rosario, D. J., McGurk, R. C., Max, C. E., et al. 2011, ApJ, 739, 44, doi: [10.1088/0004-637X/739/1/44](https://doi.org/10.1088/0004-637X/739/1/44)
- Sanders, D. B., Soifer, B. T., Elias, J. H., et al. 1988, ApJ, 325, 74, doi: [10.1086/165983](https://doi.org/10.1086/165983)
- Schawinski, K., Urry, M., Treister, E., et al. 2011, ApJL, 743, L37, doi: [10.1088/2041-8205/743/2/L37](https://doi.org/10.1088/2041-8205/743/2/L37)
- Shi, Z.-X., Luo, A. L., Comte, G., et al. 2014, Research in Astronomy and Astrophysics, 14, 1234, doi: [10.1088/1674-4527/14/10/003](https://doi.org/10.1088/1674-4527/14/10/003)

- Shlosman, I., Begelman, M. C., & Frank, J. 1990, *Natur*, 345, 679, doi: [10.1038/345679a0](https://doi.org/10.1038/345679a0)
- Silverman, J. D., Kampczyk, P., Jahnke, K., et al. 2011, *ApJ*, 743, 2, doi: [10.1088/0004-637X/743/1/2](https://doi.org/10.1088/0004-637X/743/1/2)
- Taylor, M. B. 2005, in *Astronomical Society of the Pacific Conference Series*, Vol. 347, *Astronomical Data Analysis Software and Systems XIV*, ed. P. Shopbell, M. Britton, & R. Ebert, 29
- Toomre, A., & Toomre, J. 1972, *ApJ*, 178, 623, doi: [10.1086/151823](https://doi.org/10.1086/151823)
- Turner, M. J. L., Reeves, J. N., Ponman, T. J., et al. 2001, *A&A*, 365, L110, doi: [10.1051/0004-6361:20000070](https://doi.org/10.1051/0004-6361:20000070)
- Urry, C. M., & Padovani, P. 1995, *PASP*, 107, 803, doi: [10.1086/133630](https://doi.org/10.1086/133630)
- Wada, K. 2004, *Coevolution of Black Holes and Galaxies* (Cambridge Univ. Press)
- Wang, J.-M., Chen, Y.-M., Hu, C., et al. 2009, *ApJL*, 705, L76, doi: [10.1088/0004-637X/705/1/L76](https://doi.org/10.1088/0004-637X/705/1/L76)
- Wang, L., Greene, J. E., Ju, W., et al. 2017, *ApJ*, 834, 129, doi: [10.3847/1538-4357/834/2/129](https://doi.org/10.3847/1538-4357/834/2/129)
- Wang, Q., Ding, X., Silverman, J., et al. 2025, arXiv e-prints, arXiv:2510.09059, doi: [10.48550/arXiv.2510.09059](https://doi.org/10.48550/arXiv.2510.09059)
- Wenger, M., Ochsenbein, F., Egret, D., et al. 2000, *A&AS*, 143, 9, doi: [10.1051/aas:2000332](https://doi.org/10.1051/aas:2000332)
- Yu, Q. 2002, *MNRAS*, 331, 935, doi: [10.1046/j.1365-8711.2002.05242.x](https://doi.org/10.1046/j.1365-8711.2002.05242.x)
- Yu, Q., Lu, Y., Mohayaee, R., & Colin, J. 2011
- Yue, M., Fan, X., Yang, J., & Wang, F. 2023, *AJ*, 165, 191, doi: [10.3847/1538-3881/acc2be](https://doi.org/10.3847/1538-3881/acc2be)
- Zehavi, I., Blanton, M. R., Frieman, J. A., et al. 2002, *ApJ*, 571, 172, doi: [10.1086/339893](https://doi.org/10.1086/339893)
- Zhang, Y.-W., Huang, Y., Bai, J.-M., et al. 2021, *AJ*, 162, 276, doi: [10.3847/1538-3881/ac1ce7](https://doi.org/10.3847/1538-3881/ac1ce7)
- Zwicky, F. 1956, *Ergebnisse der exakten Naturwissenschaften*, 29, 344